J Infrared Milli Terahz Waves (2025) 46:46
https://doi.org/10.1007/s10762-025-01062-8

RESEARCH

Millimeter-Wave MIMO Array with Low Interactions Between its Antenna Elements for Fifth Generation Wireless Communication Networks

Mohammad Alibakhshikenari[1,2] · Esraa Mousa Ali[3] · Iftikhar ud din[4] · Bal S. Virdee[5] · Sadiq Ullah[4] · Salahuddin Khan[6] · Chan Hwang See[7] · Takfarinas Saber[8] · Ernesto Limiti[1]

Received: 30 December 2024 / Accepted: 16 June 2025 / Published online: 30 June 2025

Abstract

This paper presents a novel, compact eight-port circular MIMO antenna system designed for millimeter-wave (mmWave) 5G communication, offering a wide impedance bandwidth and high isolation. The proposed antenna array operates over a broad measured frequency range of 25–35 GHz, achieving a 10 GHz bandwidth through a unique integration of circular and rectangular slots in the ground plane. Fabricated on a low-loss Rogers RT5880 substrate ($\varepsilon_r = 2.2$, thickness = 0.8 mm, $\tan\delta = 0.0009$), the design demonstrates excellent performance without requiring additional decoupling structures. The antenna achieves high isolation greater than 28 dB and a peak gain of 9.65 dB at 26 GHz and 28 GHz, enabling effective operation in high-attenuation mmWave environments. Compared to prior art, the presented system supports more antenna elements within a compact footprint while maintaining low Envelope Correlation Coefficient (ECC < 0.05) and high diversity gain, making it ideal for enhanced MIMO performance. Comprehensive analysis of S-parameters, radiation patterns, surface currents, and efficiency validates its suitability for next-generation 5G mmWave applications. The combination of compact geometry, high port count, wideband coverage, and exceptional isolation constitutes the core novelty of this work.

Keywords Antenna elements, multiple · Input multiple · Output (MIMO) array, millimeter · Wave (mm · Wave) domain, low interactions

Extended author information available on the last page of the article

1 Introduction

Fifth Generation (5G) wireless communication has become a central enabler of modern digital infrastructure, with widespread commercial deployments across the globe [1]. Although 5G is already operational, continuous research and development are essential to meet evolving demands in ultra-high data rates, ultra-low latency, massive device connectivity, and spectrum efficiency [2]. The exponential growth in mobile data traffic driven by services such as high-definition video streaming, cloud computing, augmented and virtual reality, and the Internet of Things (IoT) necessitates ongoing innovation in wireless system architectures [3–5].

While Fourth Generation (4G) technologies have provided reliable service, their architectural limitations restrict scalability in the face of increasing application complexity. 5G addresses these constraints through key technological pillars: enhanced Mobile Broadband (eMBB), ultra-reliable low-latency communications (URLLC), and massive Machine-Type Communications (mMTC) [6]. A foundational enabler for these features is Multiple-Input Multiple-Output (MIMO) technology, which enhances channel capacity and spectral efficiency by exploiting spatial multiplexing across multiple antennas without increasing power requirements [7, 8].

Among the various frequency allocations for 5G, the millimeter-wave (mmWave) spectrum (30–300 GHz) offers significant advantages due to its abundant bandwidth availability [9–15]. Operational bands such as 24.25–29.5 GHz (n257/n258), 37–40 GHz (n260), and 64–71 GHz (unlicensed) have been allocated by international regulatory bodies including the ITU and FCC for 5G use [16–21]. These bands are well-suited for multi-gigabit-per-second data rates but suffer from high free-space path loss, limited material penetration, and atmospheric attenuation [22–24]. To address these propagation challenges, antennas operating at mmWave must exhibit high gain, directional radiation patterns, low mutual coupling, and compact form factors [25, 26].

Despite advancements in antenna technology, designing efficient, wideband, and compact mmWave MIMO antennas remains a critical challenge. Mutual coupling between radiating elements can severely degrade isolation, radiation efficiency, and MIMO system performance [13, 14]. Furthermore, sub-6 GHz bands are saturated with legacy systems such as Wi-Fi, Bluetooth, WiMAX, and ISM applications, reinforcing the strategic value of mmWave spectrum for next-generation wireless networks [15, 16].

Several recent designs have proposed the use of complementary split-ring resonators (CSRRs), open-loop resonators (OLRs), and metamaterial-inspired techniques to enhance isolation or sensitivity [27–32]. While effective in targeted aspects, these solutions often introduce significant complexity in structure and fabrication [33–36]. For example, CSRR-loaded antennas offer dual-band performance and high sensitivity for GHz-range sensing, but their narrow operational bandwidth and two-port limitation restrict them in MIMO contexts. Defected ground structures and decouplers used in CPW-fed and S-shaped antennas can reduce mutual coupling but at the cost of increased profile or reduced radiation

gain [27, 34, 35]. Metamaterial slabs, FSS layers, and embedded resonators add functional diversity but often enlarge the antenna footprint and complicate integration [37–39].

Additionally, several recent mmWave antenna systems operating in the 20–40 GHz range have attempted to overcome these limitations using advanced electromagnetic structures. Choi et al. [40] reported a metamaterial-integrated dipole array antenna operating between 23.1–44.8 GHz, achieving high gain (11.21 dBi) using a complex 5×7 artificial magnetic conductor structure. Saleh et al. [41] enhanced antenna gain at 28 GHz using a single-layer metamaterial lens; however, the design increased the antenna height and complexity. Lin et al. [42] presented a multimode substrate-integrated gap waveguide antenna using orbital angular momentum (OAM) to enhance spatial multiplexing. While innovative, this approach introduced complex traveling-wave mechanisms and multiple layers that reduce design scalability.

In contrast, the MIMO antenna system proposed in this work presents a simplified, scalable, and fabrication-friendly alternative. The design operates over a broad mmWave range from 25 to 35 GHz, delivering an impressive 12 GHz impedance bandwidth. It features an eight-element circular patch configuration arranged diagonally to minimize mutual coupling and maintain high isolation (> 28 dB). With a compact footprint of $24\times 144\times 0.8$ mm^3, the proposed antenna system achieves a peak gain of 9.65 dB, maximum total efficiency of 92%, and excellent MIMO diversity performance characterized by an Envelope Correlation Coefficient (ECC) below 0.05.

Notably, the proposed design eliminates the need for additional decoupling structures, metamaterials, or resonator loading, enabling easier fabrication and integration into 5G hardware platforms. Unlike prior works that either address narrowband GHz sensing or focus on isolated performance improvements, this design is specifically optimized for broadband, high-capacity 5G MIMO communication within the mmWave band. Its combination of performance, simplicity, and scalability makes it a strong candidate for future mmWave wireless infrastructure and compact user-end devices.

2 Proposed Antenna Design and Methodology

The design process of the proposed eight-port MIMO antenna is divided into four main stages: single-element design, two-element MIMO configuration, four-element MIMO configuration, and final eight-element MIMO configuration. This progressive approach allows systematic evaluation of isolation, impedance bandwidth, and mutual coupling effects as the antenna scales in complexity.

2.1 Single Element Antenna

The initial antenna element is based on a circular patch structure designed on a Rogers RT/Duroid 5880 substrate, which is well known for its low dielectric loss and excellent performance at millimeter-wave frequencies. Key substrate properties are:

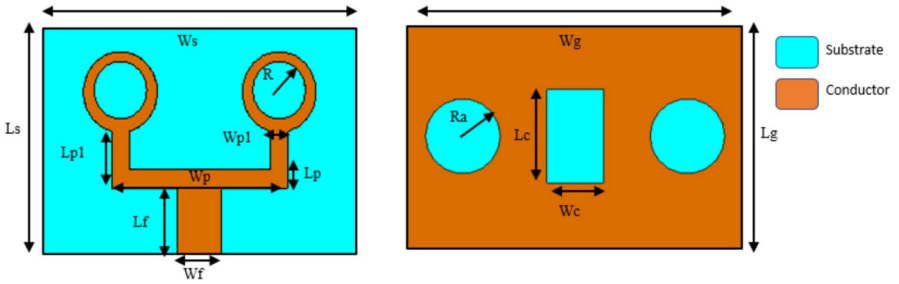

Fig. 1 Design geometry of proposed circular patch antenna array

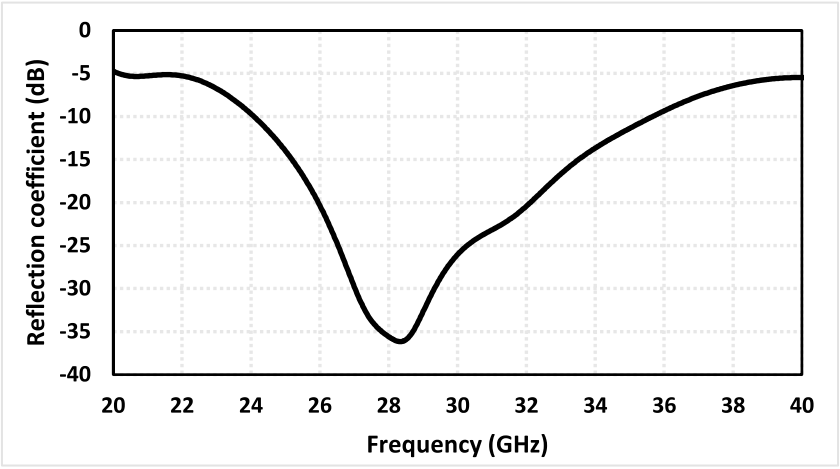

Fig. 2 Reflection coefficient of proposed two element circular patch antenna

- Dielectric constant (ε_r): 2.2 ±0.02
- Loss tangent (tanδ): 0.0009 @ 10 GHz
- Thickness: 0.8 mm

The single-element antenna, shown in Fig. 1, has a 1 ×2 array layout with dimensions of 12 ×18 ×0.8 mm^3. The ground plane is modified with circular cuts at the edges and a central rectangular slot to enhance impedance bandwidth. The antenna achieves a wide impedance bandwidth from 25 to 35 GHz (10 GHz total), covering the required mmWave range for 5G applications.

The effective radius (R_e) of the circular patch is calculated using standard microstrip patch antenna equations [43], and the physical radius is determined based on the resonant frequency as described in [44]. Figure 2 shows the reflection coefficient of proposed two element array.

$$w = \frac{V_0}{2f_r}\sqrt{\frac{2}{\varepsilon_r}} \tag{1}$$

$$L = \frac{v_0}{2f_r\sqrt{\varepsilon_{eff}}} - 2\Delta L \tag{2}$$

$$R_e = R\left\{\sqrt{1 + \frac{2H}{\pi\varepsilon rR}\left(ln\frac{\pi R}{2H} + 1.7726\right)}\right\} \tag{3}$$

$$R = \frac{F}{\left\{\sqrt{1 + \frac{2h}{\pi\varepsilon_r F}\left(\ln\frac{\pi F}{2H} + 1.7726\right)}\right\}} \tag{4}$$

$$F = \frac{8.79 \times 109}{f_r\sqrt{\varepsilon_r}} \tag{5}$$

2.2 Fabrication Process

The antenna is compatible with standard printed circuit board (PCB) fabrication techniques using the following steps:

1. Lamination of copper cladding onto the Rogers 5880 substrate.
2. Patterning of circular patches and ground slots via photolithography and chemical etching.
3. No vias or multilayer connections are required, simplifying fabrication.
4. SMA or end-launch connectors can be soldered directly to the feed lines for measurement and integration.

This process supports cost-effective manufacturing and easy scalability.

2.3 Loss Considerations at mmWave

At millimeter-wave frequencies, losses from both the substrate and the conductor become more significant. The use of Rogers 5880 substrate mitigates these losses effectively due to its low loss tangent. Additional design strategies include:

Compact geometry to reduce conductor path lengths and associated ohmic losses.
Optimized ground and patch shapes to suppress surface wave propagation.
Efficient matching techniques to minimize reflection losses.

Prototype measurements confirm high total efficiency, reaching up to 92%, which validates the design's suitability for practical mmWave applications.

2.4 Two-Element MIMO Configuration

The design is extended to a two-element MIMO configuration, with overall dimensions of 12 × 36 × 0.8 mm^3. The two identical patch elements are placed parallel to each other with a spacing of 15 mm to minimize mutual coupling, as illustrated in Fig. 3. The modified ground plane is retained for isolation enhancement.

Simulated S-parameters (shown in Fig. 4) indicate that the two-port antenna covers the full 25–35 GHz band with transmission coefficients below –20 dB, demonstrating strong isolation and minimal coupling (Table 1).

2.5 Four-Elements MIMO Configuration

To further improve channel diversity and spatial coverage, a four-element MIMO configuration is developed. The individual elements, each measuring 12 × 18 mm^2,

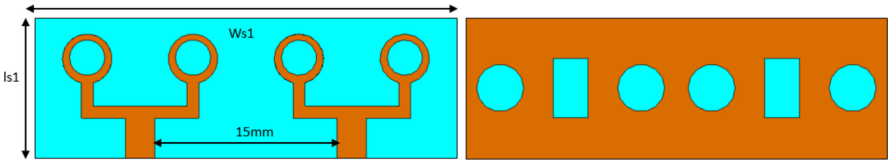

Fig. 3 Two-element multiple-input multiple-output (MIMO) antenna structure

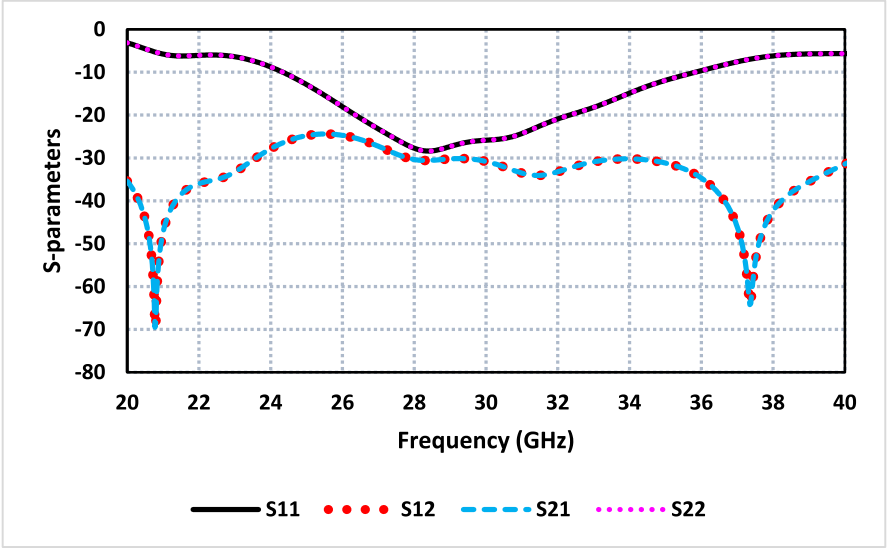

Fig. 4 S-parameters of the two-element antenna array

Table 1 Design parameters of proposed antenna

Parameters	Value (mm)	Parameters	Value (mm)
W_s	18	W_g	18
L_s	12	L_g	12
L_f	3.5	L_p	1
W_f	2.5	W_p	10
R	2.1	L_{p1}	2
R_a	2	W_{p1}	1
L_c	5	W_c	3
L_{s1}	12	Ws_1	36
L_{s2}	30	Ws_2	36
L_{s3}	24	Ws_3	144

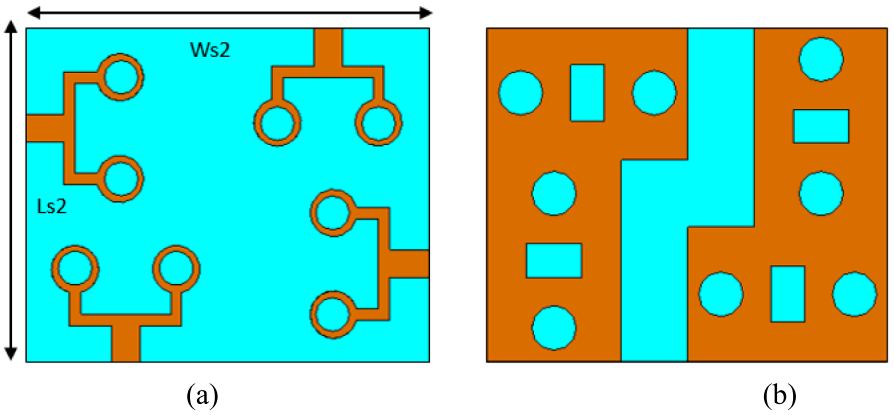

Fig. 5 Four-element MIMO antenna structure (**a**) Front View, and (**b**) Back View

are arranged in an orthogonal anti-parallel layout to form a square-like structure, as illustrated in Fig. 5.

This configuration reduces mutual coupling by increasing the physical and angular separation between elements. Isolation greater than 20 dB is achieved across the operating band. Despite the closer proximity of multiple elements, the orthogonal orientation helps maintain a low Envelope Correlation Coefficient (ECC), essential for MIMO performance. The S-parameter response of the four-element MIMO antenna structure is shown in Fig. 6.

2.6 Eight-Element MIMO Configuration

The final antenna configuration consists of eight radiating elements arranged diagonally along the top of the substrate, as shown in Fig. 7. This diagonal layout further improves isolation without requiring external decoupling structures. Ground

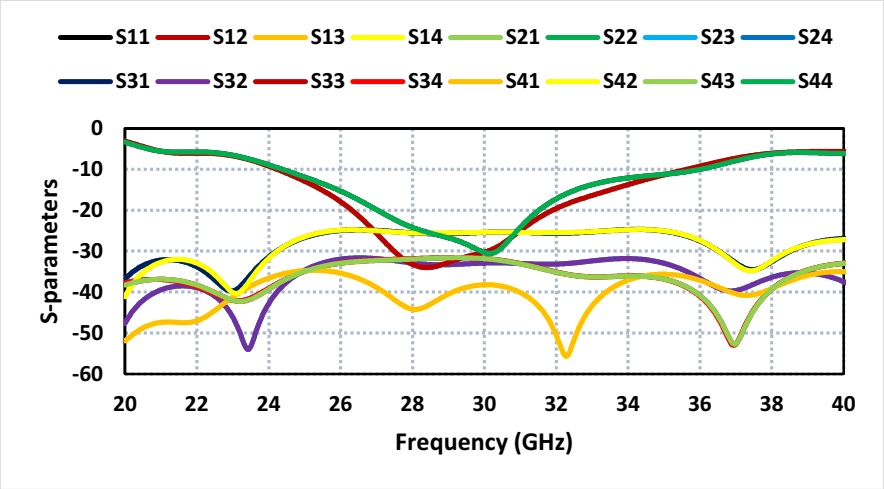

Fig. 6 S-parameter response of the four-element MIMO antenna structure

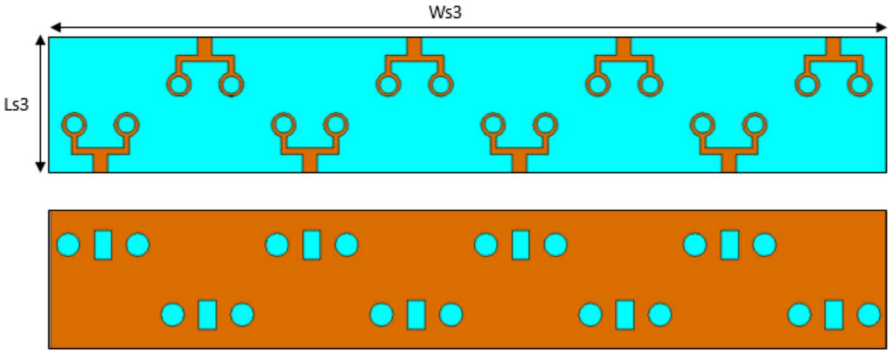

Fig. 7 Eight-element MIMO antenna structure, front and back views

plane modifications include multiple rectangular and circular slots to support wideband performance.

The final antenna has a compact overall size of $24 \times 144 \times 0.8$ mm^3. Simulated S-parameters (Fig. 8) show a reflection coefficient below –10 dB from 25 GHz to 35 GHz and transmission coefficients below –30 dB, indicating excellent inter-element isolation.

The resulting eight-port antenna achieves a 12 GHz bandwidth and supports high channel capacity, low ECC, and robust spatial diversity, making it well suited for high-throughput mmWave 5G communication systems.

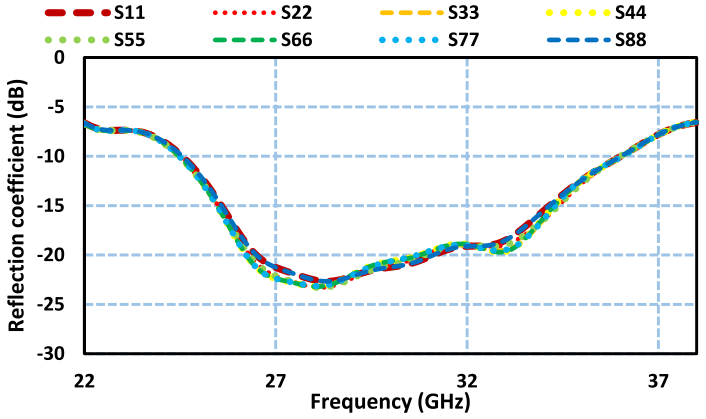

(a)

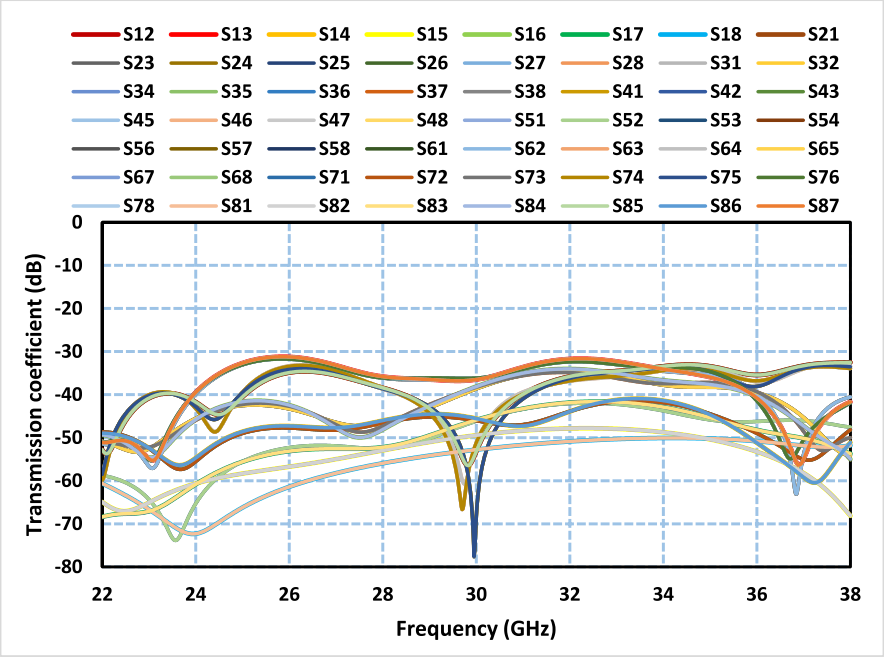

(b)

Fig. 8 **a** Reflection coefficient, and (**b**) Transmission coefficient of the proposed 8-port MIMO antenna

3 Experimental Results

To validate the simulated performance of the proposed antenna system, an eight-element MIMO prototype was fabricated on Rogers RT/Duroid 5880 substrate with a thickness of 0.8 mm and a dielectric constant of 2.2. The front and back views of

the fabricated antenna are shown in Fig. 9(a) and Fig. 9(b), respectively. The circular patch elements are arranged diagonally on the top side of the substrate, while the ground plane is etched with circular and rectangular slots on the reverse side to improve bandwidth and inter-element isolation.

The S-parameters of the fabricated antenna were measured using a Rohde & Schwarz ZVA 40 Vector Network Analyzer (VNA). Due to the symmetrical layout of the antenna, only representative S-parameters between Antenna 1 and Antenna 2 (including S_{11}, S_{21}, S_{12}, S_{13}, S_{14}, etc.) are shown in Fig. 10(a) and Fig. 10(b) for clarity.

From Fig. 10(a), it is observed that the measured reflection coefficient (S_{11} and S_{22}) lies below –10 dB across the frequency range of 25 GHz to 35 GHz, confirming a wide measured impedance bandwidth of 10 GHz. The result aligns well with the CST Studio Suite simulations, confirming good impedance matching in the fabricated design.

In Fig. 10(b), the measured transmission coefficients (S_{21} to S_{24}) remain consistently below –28 dB across the operating band, indicating excellent isolation between the antenna elements and minimal mutual coupling. The small discrepancies between simulated and measured results are attributed to fabrication tolerances, substrate handling, and connector/cable losses during measurement.

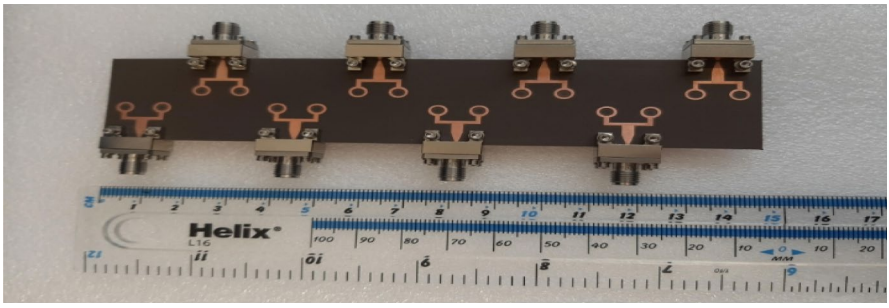

(a)

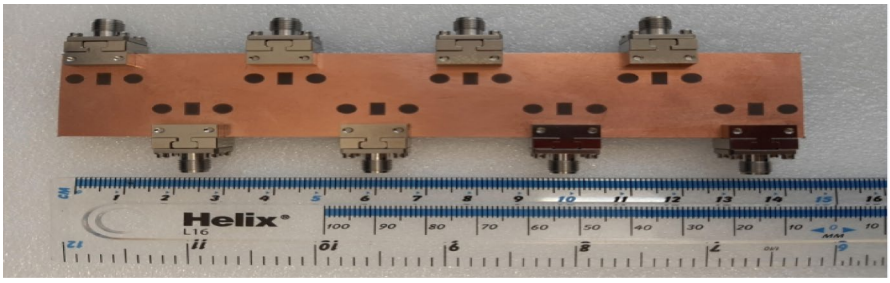

(b)

Fig. 9 **a** Front view and (**b**) Back view of the fabricated eight-element MIMO antenna system on Rogers RT/Duroid 5880 substrate

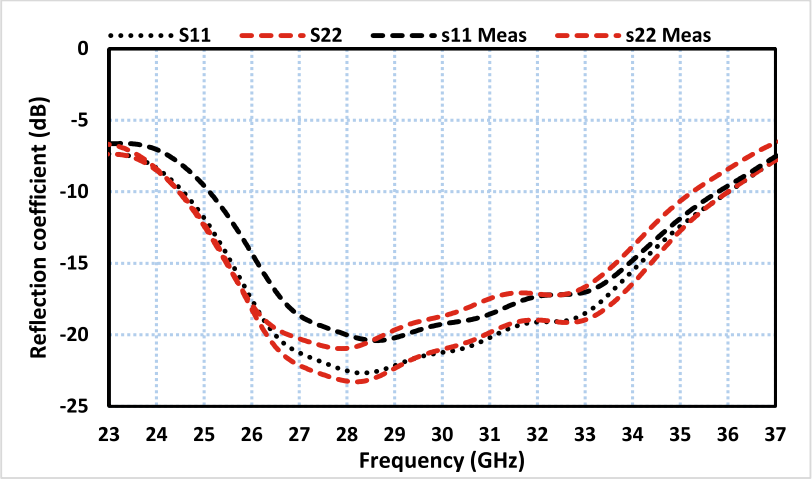

(a)

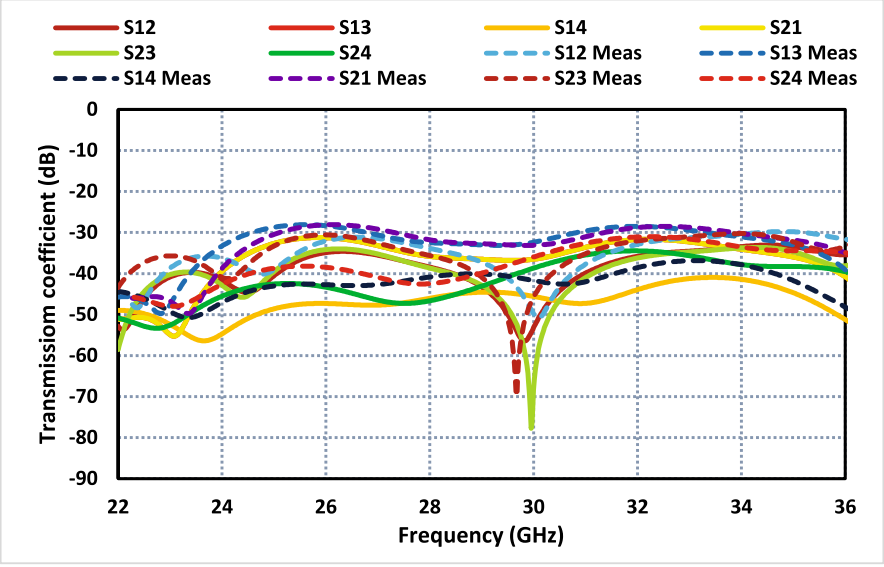

(b)

Fig. 10 **a** Simulated and measured reflection coefficients (S_{11} and S_{22}) for the 8-port MIMO antenna. **b** Simulated and measured transmission coefficients (S_{21}–S_{24}) demonstrating high isolation

To further assess antenna performance, radiation patterns were measured in an anechoic chamber at two representative frequencies: 26 GHz and 28 GHz. Simulated and measured patterns were obtained in both the E-plane and H-plane, as shown in Fig. 11(a) and Fig. 11(b).

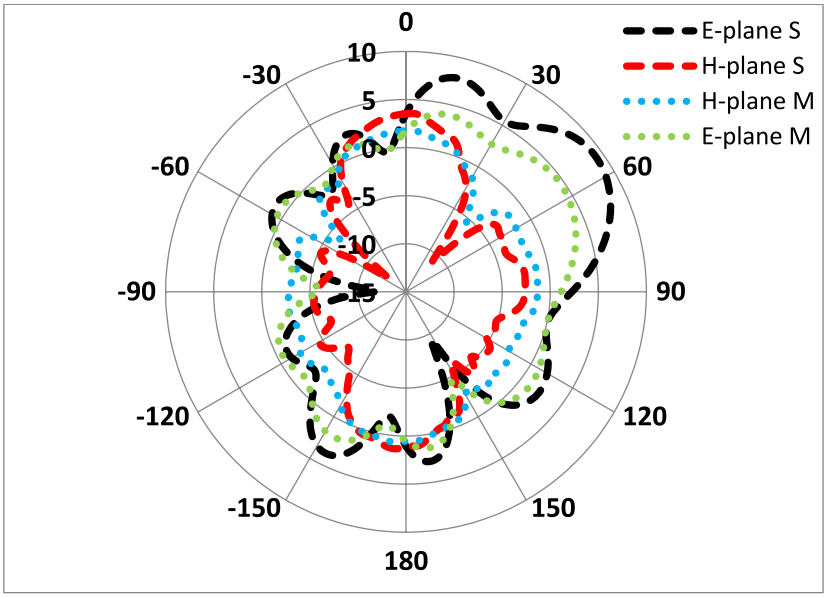

(a)

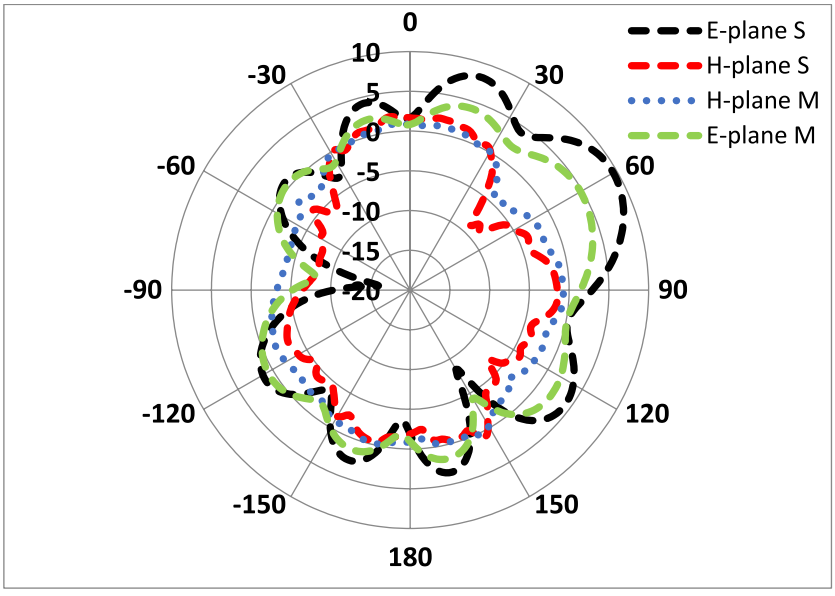

(b)

Fig. 11 Simulated and measured radiation patterns in E- and H-planes at (a) 26 GHz and (b) 28 GHz, showing consistent beam behavior in both principal planes

At 26 GHz (Fig. 11a), the E-plane shows a maximum radiation at approximately 60°, while the H-plane exhibits a main beam at 0°. The measured patterns closely follow the simulated results, with only slight variations due to practical testing conditions and connector losses.

At 28 GHz (Fig. 11b), similar radiation characteristics are observed. The E-plane again peaks around 60°, while the H-plane maintains a forward-facing main lobe near 0°. The beam shapes remain stable, and the antenna maintains directional characteristics across the operating band.

The measured radiation patterns confirm that the proposed MIMO antenna offers stable directional performance with consistent beam shapes, supporting its applicability in mmWave 5G systems requiring spatial diversity and low interference.

The measured results, including S-parameters and radiation patterns, are in good agreement with the simulated data from CST Studio Suite. This validates the antenna's broadband performance, high isolation, and directional radiation characteristics, making it a strong candidate for high-performance mmWave MIMO communication systems.

4 Gain and Efficiency of the Proposed MIMO Antenna

To evaluate the performance of the proposed antenna in terms of radiation strength and energy efficiency, both gain and total efficiency were analyzed for various configurations: single element, two-element, four-element, and eight-element MIMO systems.

4.1 Gain Analysis

Figure 12 presents the gain versus frequency plot for the antenna at different design stages beginning with a single-element configuration and evolving up to the final eight-element MIMO structure. The simulation results reveal that all configurations maintain stable gain performance across the 25–35 GHz operating band. The single-element antenna achieves a gain of approximately 8.5 dB, while the two-element and four-element configurations exhibit slight improvements due to increased aperture and constructive array effects.

The eight-element MIMO system demonstrates a further gain enhancement, with simulated gain peaking around 9.65 dB, making it highly suitable for millimeter-wave 5G applications, where high-gain directional radiation is essential to overcome free-space path loss. Additionally, the measured gain of the fabricated eight-port antenna also follows the simulated trend closely, with slight variations due to fabrication tolerances and connector losses, confirming the reliability of the simulation process.

4.2 Total Efficiency Analysis

Figure 13 shows the simulated total efficiency of each of the eight radiating elements across the operating frequency range. The efficiency curves indicate a highly uniform performance across all elements, which is critical for maintaining balanced power distribution in a MIMO system.

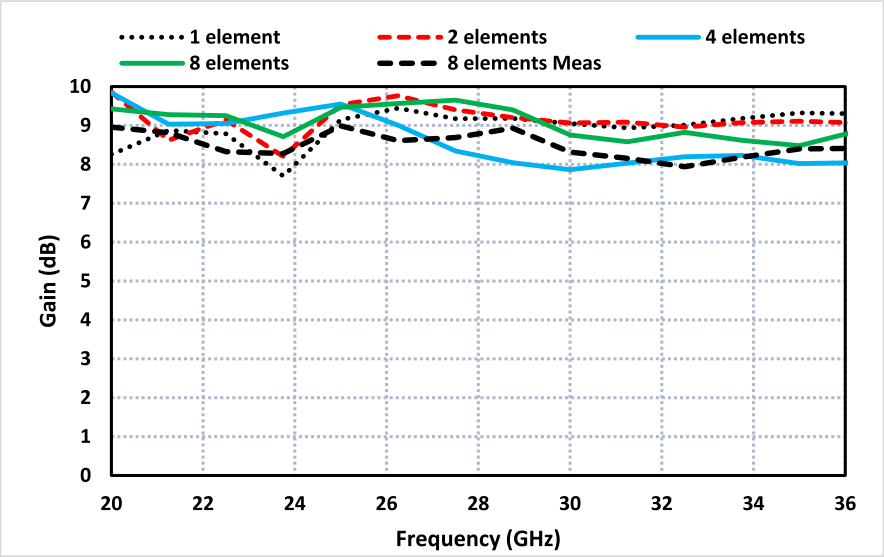

Fig. 12 Gain versus frequency comparison for 1-element, 2-element, 4-element, and 8-element MIMO configurations. Both simulated and measured gain for the 8-element antenna are shown for validation

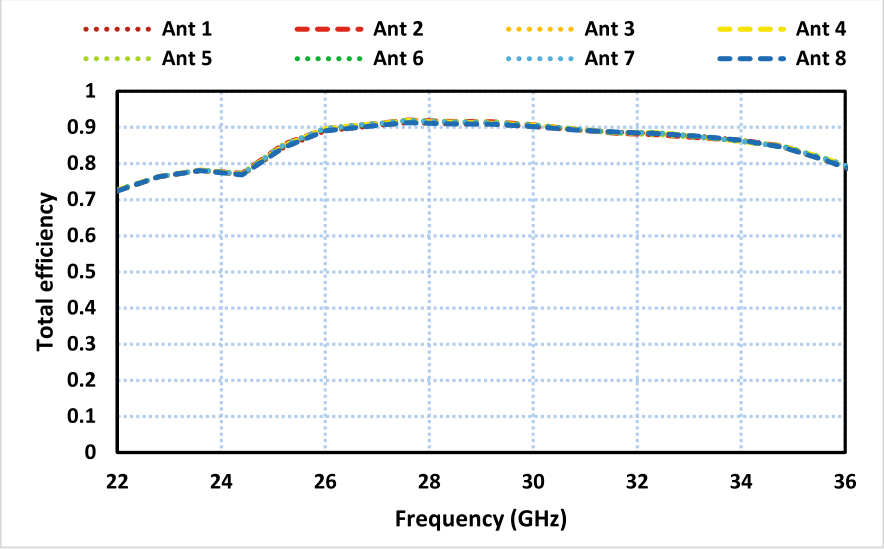

Fig. 13 Simulated total radiation efficiency of all eight MIMO antenna elements across the 25–35 GHz frequency range, showing consistent and high-efficiency performance

The antenna elements achieve maximum efficiency of 92% at 28 GHz, and maintain efficiency levels above 85% across the full 25–35 GHz band. This high efficiency is attributed to the use of low-loss Rogers RT/Duroid 5880 substrate, optimized patch and ground design, and the absence of lossy decoupling structures or complex feeding networks.

These results confirm that the proposed antenna not only offers high gain but also operates with minimal loss, supporting energy-efficient operation in high-capacity wireless communication systems.

5 MIMO Performance Parameters

To evaluate the spatial diversity performance and mutual coupling behavior of the proposed eight-port MIMO antenna system, two key metrics are analyzed: the Envelope Correlation Coefficient (ECC) and the Diversity Gain (DG). These parameters are essential for assessing the quality of signal separation and robustness in MIMO communication environments.

5.1 Envelope Correlation Coefficient (ECC)

The Envelope Correlation Coefficient (ECC) quantifies the degree of correlation between radiation patterns of different antenna elements. A low ECC indicates low mutual coupling and high diversity performance. According to MIMO performance standards, ECC values should be less than 0.5 to ensure good isolation and independent radiation behavior between ports.

The ECC is calculated using the following radiation-based formula [37]:

$$ECC = \frac{|\iint 4\pi(M_i)(\theta,\phi)) \times (M_j(\theta,\phi))d\Omega|^2}{\iint 4\pi|(M_i(\theta,\phi))|^2 d\Omega \iint 4\pi|(M_j(\theta,\phi))|^2 d\Omega} \tag{6}$$

where M_i (θ, ϕ) and M_j (θ, ϕ) represent the 3D far-field radiation patterns of antenna elements i and j, respectively, and Ω is the solid angle.

As shown in Fig. 14, the ECC values for antenna pairs (1,2) and (1,3) are extremely low below 0.0004 across the entire 25–35 GHz band. These results confirm excellent isolation and low correlation between the radiating elements, reinforcing the antenna's suitability for high-performance MIMO applications.

5.2 Diversity Gain

Diversity Gain (DG) is another crucial metric that indicates how well the MIMO system can maintain signal strength and quality under multipath propagation. It reflects the effective gain obtained from using multiple antennas instead of a single one. DG is mathematically related to ECC as follows [37]:

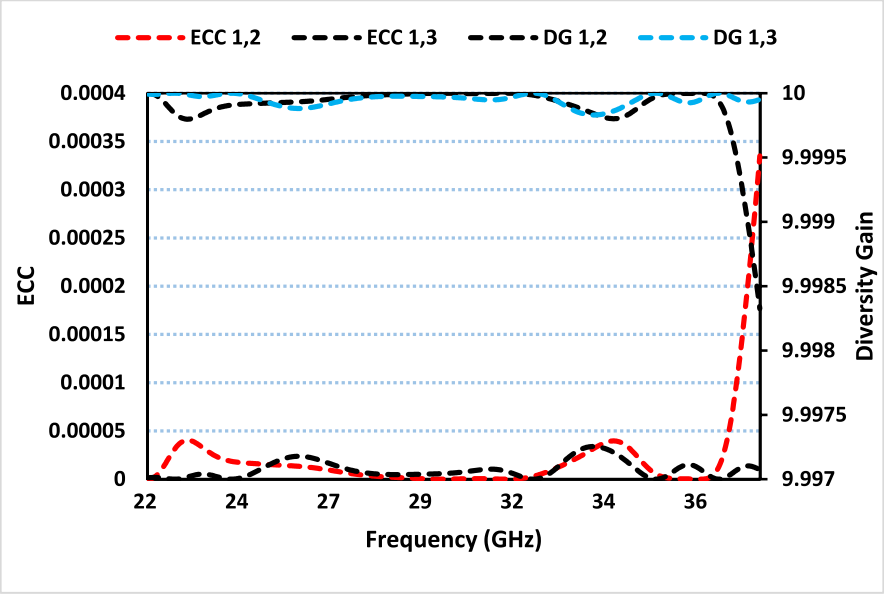

Fig. 14 Simulated Envelope Correlation Coefficient (ECC) and Diversity Gain (DG) for element pairs (1,2) and (1,3) in the eight-element MIMO system. Extremely low ECC values and near-ideal DG confirm superior spatial diversity and minimal mutual interference

$$DG = 10 \times \sqrt{\left(1 - |ECC|^2\right)} \tag{7}$$

An ideal diversity gain value approaches 10 dB, indicating minimal power loss due to signal correlation.

As depicted in Fig. 14, the calculated DG for element pairs (1,2) and (1,3) is consistently greater than 9.997 dB across the entire frequency band, demonstrating the excellent diversity performance of the proposed system.

6 Comparison with State-of-the-Art

To highlight the performance and uniqueness of the proposed eight-port MIMO antenna, a detailed comparison is provided in Table 2 against several recently published MIMO antenna systems. The comparison focuses on critical performance metrics including the number of ports, operating bandwidth, peak gain, physical dimensions, inter-element isolation, and Envelope Correlation Coefficient (ECC).

From the comparison, it is evident that the proposed antenna offers a superior balance of wide bandwidth, high gain, compact footprint, and strong MIMO performance all essential for modern millimeter-wave (mmWave) 5G communication systems.

Table 2 Comparison of the proposed antenna with other state-of-the-art MIMO antenna systems in terms of key performance metrics

Ref	Ports	Bandwidth (GHz)	Max. Gain (dB)	Size (mm^3)	Isolation (dB)	ECC
[28]	4	25–40	7.2	158 ×77.8	> 17	< 0.03
[29]	-	24–28	7.4	30 ×30.5 × 0.508	-	-
[30]	2	2.6–13	0.76–6.02	66.8 × 40 × 0.8	> 15	< 0.02
[31]	4	26–29.5	14	19 × 19 × 0.76	> 20	< 0.015
[32]	4	25.5–29.6	8.3	30 ×35 × 0.76	> 10	< 0.01
[33]	4	26–30	8	25 × 15	> 20	< 0.001
[34]	4	25–40	7	24 × 24 ×0.254	26	< 0.05
[35]	4	23–40	10	80 × 80	22	< 0.01
[36]	4	36.83–40	6.5	47.4 × 32.5 ×0.51	45	< 0.05
[37]	2	27–29	8.75	18 × 38 × 0.8	64	< 0.005
[38]	1	3.2–14	8.1	62.5 × 62.5 × 25	-	-
[39]	1	3–15	8.1	62.5 × 62.5 × 25	-	-
This Work	8	25–35	9.65	24 × 144 × 0.8	> 20	< 0.05

The key distinguishing features of the proposed design are as follows:

- Higher number of ports (8): Most referenced designs support only 2 or 4 ports. The proposed antenna supports 8 ports, which significantly increases spatial multiplexing and channel capacity—vital for dense urban 5G deployments and beamforming.
- Wide operating bandwidth (25–35 GHz): Several designs (e.g., [29, 31, 32]) cover narrower bands such as 25–28 GHz or 26–29.5 GHz. The proposed antenna achieves a 12 GHz bandwidth, allowing it to support multiple 5G bands simultaneously and enabling higher data throughput.
- High peak gain (9.65 dB): The gain is comparable to or higher than most of the referenced works, with only [31] reporting a higher gain (14 dB) but with fewer ports and a smaller band. The proposed gain ensures effective signal transmission over mmWave channels that suffer from high path loss.
- Compact and scalable design (24 ×144 ×0.8 mm^3): Despite offering more ports and wide bandwidth, the antenna maintains a slim profile using a diagonal placement strategy and avoids complex decoupling or metamaterial structures. Designs like [35] (80 ×80 mm^2) occupy a larger footprint with fewer ports.
- Strong isolation and low ECC: The proposed design achieves inter-element isolation > 20 dB and ECC < 0.05, indicating excellent diversity performance and low mutual coupling. This ensures high-quality MIMO communication with reduced signal correlation and interference.

Overall, the proposed antenna demonstrates a well-optimized trade-off between performance metrics and practical implementation constraints. It outperforms or competes favorably with other designs in all key categories and is well suited for integration into compact mmWave 5G systems requiring high capacity and wideband support.

7 Conclusion

In this work, a novel eight-element MIMO antenna system has been developed for 5G mmWave applications, operating effectively across a wide frequency range of 25–35 GHz. The proposed design introduces a diagonally arranged antenna configuration on a compact substrate footprint of $24 \times 144 \times 0.8$ mm^3, facilitating low mutual coupling without the need for external decoupling structures. This spatial arrangement significantly enhances isolation performance, consistently achieving values greater than 28 dB across the entire operating bandwidth outperforming many contemporary designs.

One of the key innovations of this work lies in the methodical evolution from a single-element antenna to a full eight-element MIMO array, enabling enhanced channel capacity and data throughput while maintaining structural simplicity and fabrication feasibility. The antenna achieves a broad impedance bandwidth of 10 GHz and a high peak gain of 9.65 dB, supported by a maximum total efficiency of 92%, making it highly effective in overcoming propagation challenges such as atmospheric attenuation that are prevalent in mmWave bands.

Furthermore, rigorous evaluation of essential MIMO performance metrics, including Envelope Correlation Coefficient (ECC < 0.05) and Diversity Gain, demonstrates strong spatial and pattern diversity, essential for reliable multi-stream transmission in 5G systems. The measured results closely align with simulation data, affirming the robustness and practical viability of the design.

The novelty of this work is underscored by its ability to integrate high port-count MIMO functionality with wideband operation, compact size, high isolation, and superior radiation performance all without sacrificing design simplicity or requiring complex isolation enhancement techniques. These attributes establish the proposed antenna as a strong candidate for high-performance 5G mmWave communication systems and future wireless networks demanding compact, high-efficiency MIMO solutions.

.

Author Contribution Conceptualization, M.A., E.M.A., I.U.D., B.V., C.H.S., T.S., E.L.; methodology, M.A., E.M.A., I.U.D., B.V., S.U.; software, M.A., E.M.A., I.U.D., B.V.; validation, M.A., E.M.A., I.U.D., B.V., S.U., N.A.A., C.H.S., T.S., E.L.; formal analysis, M.A., E.M.A., B.V., C.H.S., T.S., and E.L.; investigation, M.A., I.U.D., B.V., N.A.A., C.H.S.; resources, M.A., E.M.A., I.U.D., B.V., S.U., N.A.A., C.H.S., T.S., E.L.; data curation, M.A., E.M.A., I.U.D., B.V., C.H.S.,; writing—original draft preparation, M.A., I.U.D., B.V.; writing—review and editing, M.A., E.M.A., I.U.D., B.V., S.U., N.A.A., C.H.S., T.S., and E.L.; visualization, M.A., I.U.D., B.V., T.S., and E.L.; supervision, T.S., E.L.; project administration, M.A.; funding acquisition, M.A.. All authors have read and agreed to the published version of the manuscript.

Data Availability All data generated or analysed during this study are included in this published article.

Declarations All of the figures, materials, and data within the manuscript are original and owned by authors.

Competing interests The authors declare no competing interests.

References

1. N. Qasem, "Measurement and Simulation for Improving Indoor Wireless Communication System Performance at 2.4 GHz by Modifying the Environment," IEEE Access, vol. 12, pp. 96660-96671, 2024.
2. M. Z. Iskandarani, "Investigation of Energy Consumption in WSNs Within Enclosed Spaces Using Beamforming and LMS (BF-LMS)", IEEE Access, vol. 12, pp. 63932-63941, 2024.
3. Sharaf, M.H.; Zaki, A.I.; Hamad, R.K.; Omar, M.M.M. A novel dual-band (38/60 GHz) patch antenna for 5G mobile handsets. Sensors 2015, 20, 2541.
4. Haroon, M. S.; Muhammad, F.; Abbas, G.; Abbas, Z.H.; Kamal, A.;Waqas, M.; Kim, S. Interference Management in Ultra-Dense 5G Networks with Excessive Drone Usage. IEEE Access 2020, 1–10.
5. Khan, J.; Sehrai, D.A.; Ali, U. Design of dual band 5G antenna array with SAR analysis for future mobile handsets. J. Electr. Eng. Technol. 2019, 14, 809–816.
6. Pervez, M.M.; Abbas, Z.H.; Muhammad, F.; Jiao, L. Location-based coverage and capacity analysis of a two tier HetNet. IET Commun. 2017, 11, 1067–1073.
7. Sun, L.; Li, Y.; Zhang, Z.; Feng, Z. Wideband 5G MIMO antenna with integrated orthogonal-mode dual-antenna pairs for metal-rimmed smartphones. IEEE Trans. Antennas Propag. 2020, 68, 2494–2503.
8. Abdullah, M.; Kiani, S.H.; Iqbal, A. Eight element multiple-input multiple-output (MIMO) antenna for 5G mobile applications. IEEE Access 2019, 7, 134488–134495.
9. Abirami, M. A review of patch antenna design for 5G. In Proceedings of the 2017 IEEE International Conference on Electrical, Instrumentation and Communication Engineering (ICEICE), Karur, India, 27–28 April 2017; IEEE: Piscataway, NJ, USA, 2017; pp. 1–3.
10. Haraz, O.M. Broadband and 28/38-GHz dual-band printed monopole/elliptical slot ring antennas for the future 5G cellular communications.J. Infrared Millim. Terahertz Waves 2016, 37, 308–317.
11. Şeker, C.; Güneşer, M.T. A single band antenna design for future millimeter wave wireless communication at 38 GHz.Eur. J. Eng. Form. Sci. 2018, 2, 35–39.
12. Hong, W.; Baek, K.H.; Ko, S. Millimeter-wave 5G antennas for smartphones: Overview and experimental demonstration. IEEE Trans. Antennas Propag. 2017, 65, 6250–6261.
13. Wang, F.; Duan, Z.; Wang, X.; Zhou, Q.; Gong, Y. High isolation millimeter-wave wideband MIMO antenna for 5G communication. Int. J. Antennas Propag. 2019, 2019, 4283010.
14. Abdullah, M.; Kiani, S.H.; Abdulrazak, L.F.; Iqbal, A.; Bashir, M.A.; Khan, S.; Kim, S. High-performance multiple-input multiple-output antenna system for 5G mobile terminals. Electronics 2019, 8, 1090.
15. Khan, J.; Sehrai, D.A.; Khan, M.A.; Khan, H.A.; Ahmad, S.; Ali, A.; Arif, A.; Memon, A.A.; Khan, S. Design and performance comparison of rotated Y-shaped antenna using different metamaterial surfaces for 5G mobile devices. Comput. Mater. Contin. 2019, 60, 409–420.
16. Niu Y, Li Y, Jin D, Su L, Vasilakos AV. A survey of millimeter wave communications (mmWave) for 5G: opportunities and challenges. Wireless Netw 2015; 21:2657–2676. https://doi.org/10.1007/s11276-015-0942-z.
17. J. L. Kuo, Y. F. Lu, T. Y. Huang, Y. L. Chang, Y. K. Hsieh, P. J. Peng, I. C. Chang, T. C. Tsai, K. Y. Kao, W. Y. Hsiung, J. Wang, Y. Hsu, K. Y. Lin, H. C. Lu, Y. C. Lin, L. H. Lu, T. W. Huang, R. B.

Wu, and H. Wang, "60-GHz four-element phased-array transmit/receive system-in-package using phase compensation techniques in 65-nm flip-chip CMOS process,"IEEE Trans. Microw. Theory Tech., vol. 60, no. 3, pp. 743–756, Mar. 2012.
18. Wang, C.-X., Haider, F., Gao, X., et al.: 'Cellular architecture and keytechnologies for 5G wireless communication networks', Commun. Mag., 2014, 52, (2), pp. 122–130.
19. Hussain, R., Alreshaid, A.T., Podilchak, S.K., et al.: 'Compact 4G MIMO antenna integrated with a 5G array for current and future mobile handsets', IET Microw. Antennas Propag. 2017, 11, (2), pp. 271–279.
20. Li, Y., Wang, C., Yuan, H., et al.: 'A 5G MIMO antenna manufactured by 3-D printing method', IEEE Antennas Wirel. Propag. Lett., 2017, 16, pp. 657–660.
21. Di, W., Cheung, S. W., Yuk, T. I., et al.: 'A planar MIMO antenna for mobile phones'. Proc. PIERS, 2013, pp. 1150–1152.
22. Wang, P.; Li, Y.; Song, L.; Vucetic, B. Multi-gigabit millimeter waves wireless communications for 5G: From fixed access to cellular networks. IEEE Commun. Mag. 2015, 53, 168–178.
23. Sulyman, A.I.; Alwarafy, A.; MacCartney, G.R.; Rappaport, T.S.; Alsanie, A. Directional radio propagationpath loss models for millimeter-wave wireless networks in the 28-, 60-, and 73-GHz bands. IEEE Trans. Wirel.Commun. 2016, 15, 6939–6947.
24. Shayea, I.; Rahman, T.A.; Azmi, M.H.; Islam, M.R. Real measurement study for rain rate and rain attenuation conducted over 26 GHz microwave 5G link system in malaysia. IEEE Access 2018, 6, 19044–19064.
25. Roh, W.; Seol, J.Y.; Park, J.; Lee, B.; Lee, J.; Kim, Y.; Cho, J.; Cheun, K.; Aryanfar, F. Millimeter-wavebeamforming as an enabling technology for 5G cellular communications: Theoretical feasibility and prototype results. IEEE Commun. Mag. 2014, 52, 106–113.
26. Khalily, M.; Tafazolli, R.; Xiao, P.; Kishk, A.A. Broadband mm-Wave microstrip array antenna with improved radiation characteristics for different 5G applications. IEEE Trans. Antennas Propag. 2018, 66, 4641–4647.
27. Jilani, S.F.; Alomainy, A. Millimetre-wave T-shaped MIMO antenna with defected ground structures for 5G cellular networks.IET Microwaves Antennas Propag. 2018, 12, 672–677.
28. Abbas, E.A.; Ikram, M.; Mobashsher, A.T.; Abbosh, A. MIMO antenna system for multi-band millimeter-wave 5G and wideband 4G mobile communications. IEEE Access 2019, 7, 181916–181923.
29. Jiang, H.; Si, L.; Hu, W.; Lv, X. A symmetrical dual-beam bowtie antenna with gain enhancement using metamaterial for 5G MIMO applications. IEEE Photonics J. 2019, 11, 1–9.
30. Patre, S.R.; Singh, S.P. Broadband multiple-input–multiple-output antenna using castor leaf-shaped quasi-self-complementary elements. In IET Microwaves, Antennas & Propagation; IET: Hertford, UK, 2016; Volume 10, pp. 1673–1681.
31. Hussain, N.; Jeong, M.; Park, J.; Kim, N. A broadband circularly polarized fabry-perot resonant antenna using a single-layered PRS for 5G MIMO applications. IEEE Access 2019, 7, 42897–42907.
32. Khalid, M.; Iffat Naqvi, S.; Hussain, N.; Rahman, M.; Mirjavadi, S.S.; Khan, M. J.; Amin, Y. 4-port MIMO antenna with defected ground structure for 5G millimeter wave applications. Electronics 2020, 9, 71.
33. Rahman, S.; Ren, X.c.; Altaf, A.; Irfan, M.; Abdullah, M.; Muhammad, F.; Anjum, M.R.; Mursal, S.N.F.; AlKahtani, F.S. Nature inspired MIMO antenna system for future mmWave technologies. Micromachines 2020, 11, 1083.
34. Khan, M.A., Al Harbi, A.G., Kiani, S.H., Nordin, A.N., Munir, M.E., Saeed, S.I., Iqbal, J., Ali, E.M., Alibakhshikenari, M. and Dalarsson, M., 2022. mmWave Four-element MIMO antenna for future 5G systems. *Applied Sciences*, *12*(9), p.4280.
35. Sehrai, D.A.; Abdullah, M.; Altaf, A.; Kiani, S.H.; Muhammad, F.; Tufail, M.; Irfan, M.; Glowacz, A.; Rahman, S. A Novel High Gain Wideband MIMO Antenna for 5G Millimeter Wave Applications. Electronics 2020, 9, 1031.
36. Sehrai, D.A., Asif, M., Shoaib, N., Ibrar, M., Jan, S., Alibakhshikenari, M., Lalbakhsh, A. and Limiti, E., 2021. Compact quad-element high-isolation wideband MIMO antenna for mm-wave applications. *Electronics*, *10*(11),1300..]
37. Din, I.U., Ullah, S., Mufti, N., Ullah, R., Kamal, B. and Ullah, R., 2023. Metamaterial-based highly isolated MIMO antenna system for 5G smartphone application. *International Journal of Communication Systems*, p.e5392.

38. Din, I.U., Ullah, S., Naqvi, S.I., Ullah, R., Ullah, S., Ali, E.M. and Alibakhshikenari, M., 2022. Improvement in the Gain of UWB Antenna for GPR Applications by Using Frequency-Selective Surface. *International Journal of Antennas and Propagation*, *2022*.
39. I. U. Din *et al.*, "A Novel Compact Ultra-Wideband Frequency-Selective Surface-Based Antenna for Gain Enhancement Applications," *Journal of Electromagnetic Engineering and Science*, vol. 23, no. 2, pp. 108–121, Mar. 2023.
40. Choi, D., Sufian, M. A., Lee, J., Awan, W. A., Choi, Y., & Kim, N. (2024). Advanced Metamaterial-Integrated Dipole Array Antenna for Enhanced Gain in 5G Millimeter-Wave Bands. *Applied Sciences*, 14(19), 9138. https://doi.org/10.3390/app14199138
41. Saleh, C. M., Almajali, E., Jarndal, A., Yousaf, J., Aljaafreh, S. S., & Amaya, R. E. (2023). Wideband 5G antenna gain enhancement using a compact single-layer millimeter wave metamaterial lens. *IEEE Access*, 11, 14928–14942.
42. Lin, Q.-H., Hou, D., Wang, L., Chen, P., & Luo, Z. (2024). A Millimeter-Wave Broadband Multi-Mode Substrate-Integrated Gap Waveguide Traveling-Wave Antenna with Orbit Angular Momentum. *Sensors*, 24(4), 1184.
43. I. Ud din, S. Ullah, and M. R. Akram, "UWB monopole antenna backed by single layer FSS for high gain antenna applications," *2022 Workshop on Microwave Theory and Techniques in Wireless Communications (MTTW)*, Oct. 2022, pp. 119–122.
44. ud Din, I., Ullah, S., Ullah, K., Fawad, Y., Ahmad, I., Ullah, S. and Habib, U., 2020, November. Circular monopole ultra-wideband (UWB) antenna with reconfigurable band-notched characteristics. In *2020 IEEE 23rd International Multitopic Conference (INMIC)* (pp. 1–6). IEEE.

Authors and Affiliations

Mohammad Alibakhshikenari[1,2] · Esraa Mousa Ali[3] · Iftikhar ud din[4] · Bal S. Virdee[5] · Sadiq Ullah[4] · Salahuddin Khan[6] · Chan Hwang See[7] · Takfarinas Saber[8] · Ernesto Limiti[1]

✉ Mohammad Alibakhshikenari
alibakhshikenari@ing.uniroma2.it; limiti@ing.uniroma2.it

✉ Chan Hwang See
c.see@napier.ac.uk

Esraa Mousa Ali
e.ali@ammanu.edu.jo

Iftikhar ud din
iftikharuddin114@gmail.com

Bal S. Virdee
b.virdee@londonmet.ac.uk

Sadiq Ullah
sadiqullah@uetmardan.edu.pk

Salahuddin Khan
drskhan@ksu.edu.sa

Takfarinas Saber
takfarinas.saber@universityofgalway.ie

Ernesto Limiti
limiti@ing.uniroma2.it

[1] Department of Electronics Engineering, University of Rome "Tor Vergata", 00133 RM Rome, Italy

[2] Department of Electrical and Electronics Engineering, Dogus University, 34775 Umraniye Istanbul, Türkiye

[3] Communications and Computer Engineering Department, Al-Ahliyya Amman University, Amman 19111, Jordan

[4] Telecommunication Engineering Department, University of Engineering and Technology, Mardan 23200, Pakistan

[5] Center for Communications Technology, London Metropolitan University, London N7 8DB, UK

[6] Department of Electrical Engineering, University of Hafr Al Batin, 39524 Hafr Al Batin, Saudi Arabia

[7] School of Engineering and the Built Environment, Edinburgh Napier University, 10 Colinton Rd, Edinburgh EH10 5DT, U.K.

[8] Lero the Research Ireland Centre for Software, School of Computer Science, University of Galway, H91 TK33 Galway, Ireland